

## AN ABSTRACT OF THE THESIS OF

Peggy A. Lopez for the degree of Master of Science in Physics presented on  
February 19, 1997. Title: The Three-Grating Optical Interferometer used as a  
Monitoring and Stabilization Device for an Atomic Interferometer

Redacted for Privacy

Abstract approved: \_\_\_\_\_

David H. McIntyre

The three-grating optical interferometer is studied to identify restrictions on alignment and improve stability. A description of the way a three-grating interferometer works is given as well as a method for proper set up. The overall power loss through the three gratings is measured and can be used to estimate the amount of atoms that will be detected at the output of the atomic interferometer. Criteria are developed for misalignment affects. Equations are presented for spacing and rotation limitations which can then be applied to the atomic interferometer. A stabilization technique is developed using a servo system. The elimination of low frequency inertial noise is accomplished.

**The Three-Grating Optical Interferometer used as a Monitoring and Stabilization  
Device for an Atomic Interferometer**

**by**

**Peggy A. Lopez**

**A THESIS**

**submitted to**

**Oregon State University**

**in partial fulfillment of  
the requirements for the  
degree of**

**Master of Science**

**Presented February 19, 1997  
Commencement June 1997**

Master of Science thesis of Peggy A. Lopez presented on February 19, 1997

APPROVED:

Redacted for Privacy

---

Major Professor, representing Physics

Redacted for Privacy

---

Chair of Department of Physics

Redacted for Privacy

---

Dean of Graduate School

I understand that my thesis will become part of the permanent collection of Oregon State University libraries. My signature below authorizes release of my thesis to any reader upon request.

Redacted for Privacy

---

✓ Peggy A. Lopez, Author

## Acknowledgments

I would first like to thank David McIntyre my thesis professor for assisting me in getting finished with my thesis and being so patient with me during the editing process. I would like to thank all the faculty of the Physics Department for allowing me to come back after being out of school for over two years and completing my degree.

Thanks to my co-workers at Videx, Rich Granvold and Kirk Rensmeyer for listening to me go over my ideas in my head and helping with the proofreading process. A special thank you goes to my family; my husband Randy, my son Raven, and my daughter Nikita for understanding when I had to go out sometimes late at night to work on my thesis, or leaving me alone at home to get some work done. A special mention goes to my parents who are no longer here to see me finally complete this event in my life, but are with me in spirit.

## Table of Contents

	<u>Page</u>
1: Introduction .....	1
2: Three-Grating Interferometer Specifications .....	4
2.1 Intensity Profile of a Grating and Power Considerations .....	4
2.2 How the Three-Grating Interferometer Works .....	6
2.3 Alignment Specifications .....	7
2.3.1 Separating the Correct Beams .....	7
2.3.2 Grating Separation and Rotation Limitations .....	9
3: Stabilization Using a Servo System .....	15
3.1 Stabilization Criteria .....	15
3.2 The Servo System .....	15
4: Results of Stabilization .....	20
4.1 Data Acquisition Techniques .....	20
4.2 Analysis of the Noise .....	20
4.3 Low Frequency Noise Reduction .....	22
5: Conclusions .....	26
Bibliography .....	28

## List of Figures

<u>Figure</u>	<u>Page</u>
1.1 The Bonse-Hart design for the three-grating interferometer .....	2
2.1 Intensity pattern for a multi-slit grating .....	5
2.2 A multi-slit diffraction grating .....	8
2.3 Rotation angles for the three degrees of freedom .....	10
2.4 Z axis translation of the third grating .....	11
2.5 Y axis rotation ( $\beta$ rotation) limitations .....	13
3.1 Diagram of the three-grating interferometer servo system .....	17
3.2 Schematic diagram of the servo circuit .....	18
3.3 Pictorial view of the servo circuit locking technique .....	19
4.1 Servo circuit offset monitor signal .....	21
4.2 Frequency spectra of the servo system output .....	24
4.3 Frequency spectra with the servo circuit on and off .....	25

# **The Three-Grating Optical Interferometer used as a Monitoring and Stabilization Device for an Atomic Interferometer**

## **Chapter 1**

### **Introduction**

Ever since Thomas Young diffracted light through a double slit in 1802, the interest in the interference of light waves has continued to grow. Interferometers using diffraction gratings as beam splitters date back to the early 1900's when Barus described several interferometer designs using diffraction gratings [Chang *et al.*, 1975]. In 1923 de Broglie hypothesized that matter could also act as a wave and thus be diffracted. This led to the use of atoms as a source for interferometers.

With the advancement of technology comes a new age in interferometry. Many experiments have shown that electrons [Marton 1952], neutrons [Rauch 1987], as well as atoms [Keith *et al.*, 1988] can be diffracted and recombined to create an interference pattern. Many devices have been developed to enable this new area of atom optics to evolve. Diffraction of neutrons has been accomplished with the use of crystal planes of silicon [Bonse and Hart 1965], while atoms have been diffracted using standing-wave laser gratings [Martin *et al.*, 1988] as well as amplitude transmission gratings [Keith *et al.*, 1988].

The Bonse-Hart interferometer is very desirable for use with atoms. Its basic design is shown in Figure 1.1 and demonstrates an easy way to separate low order diffracted beams and recombine them. With modern technology, amplitude transmission gratings can be produced with small spacings in the nanometer regime suitable for atomic interferometry.

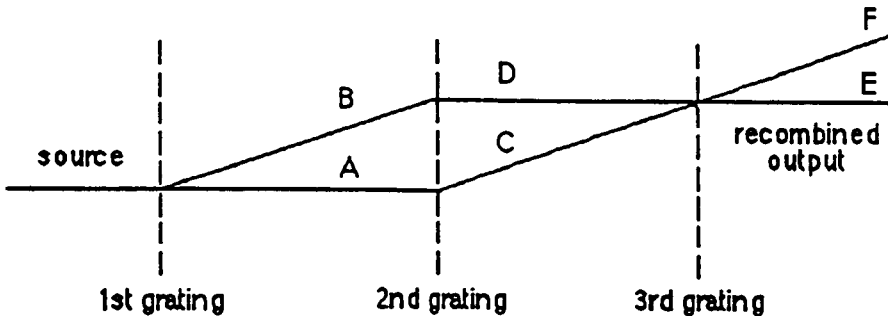


**Figure 1.1** The Bonse-Hart design for the three-grating interferometer. Path A is the 0th order maxima from the first grating, path B is the -1st order maxima from the first grating, path C is the -1st order maxima from the second grating, and path D is the +1st order maxima from the second grating. Paths E and F are the two main output beams used for detection of proper alignment. Only a few diffracted orders are shown and the ordering of the maxima will be explained in chapter 2.

The main objective of this thesis is to investigate the three-grating interferometer which will be used as a measuring device for an atomic beam of Rubidium atoms created by our group. An optical version of the three-grating interferometer will be placed along side the atomic version to aid in stabilization of the three grating positions. In order to fully understand what will happen when the atomic beam passes through the three-grating interferometer, we must first familiarize ourselves with the optical version. In doing so, we will verify alignment constraints and test the stabilization of the grating position.

In chapter 2 a theoretical intensity profile of a multi-slit grating will be described and experimental power readings of the input and final output of the three-grating interferometer will be presented. It also includes a full description of the three-grating interferometer, a method for separating the correct ordered beams, and misalignment constraints. Stabilization of the three-grating interferometer and a description of the servo system will be discussed in Chapter 3. The results of stabilization will be presented in Chapter 4. This

chapter will include methods of data collection, analysis of the data, and a description of the low frequency noise eliminated by using the servo system.

Chapter 5 will present the conclusions of this thesis.

## Chapter 2

### Three-Grating Interferometer Specifications

#### 2.1 Intensity Profile of a Grating and Power Considerations

In order to fully understand how each grating of the three-grating interferometer works, a short description of a multi-slit grating will be discussed. An intensity pattern is created behind the first grating interface and only certain ordered beams are allowed to proceed through to the second grating with each beam generating an intensity pattern of its own (see Figure 2.1). The ordered beams decrease in power as they proceed through the three-grating interferometer and thus measurements of these beams at each grating will aid in determining what fraction of the input beam will eventually be detected behind the third grating. For a multi-slit grating, the intensity is given by

$$I(\theta) = I_0 \left( \frac{\sin \beta}{\beta} \right)^2 \left( \frac{\sin N\alpha}{\sin \alpha} \right)^2 \quad (2.1)$$

where  $I_0$  is the intensity in the  $\theta = 0$  direction for each individual slit with  $\beta = (K b/2) \sin \theta$ ,  $\alpha = (K a/2) \sin \theta$ ,  $K = 2\pi/\lambda$ ,  $a$  is the grating spacing,  $b$  is the grating width, and  $N$  is the number of slits [Hecht & Zajac 1979]. Principal maxima occur when

$$\frac{\sin N\alpha}{\sin \alpha} = N, \quad \alpha = 0, \pm \pi, \pm 2\pi, \dots \quad (2.2)$$

thus

$$a \sin \theta_m = m\lambda, \quad m = 0, \pm 1, \pm 2, \dots \quad (2.3)$$

where  $\theta_m$  is the angle of diffraction for each ordered maxima and  $m$  is the order number. In addition to the principle maxima, there are  $N-2$  secondary maxima between the principal maxima. However, these subsidiary maxima are very low

in intensity compared to the principal maxima so they only need to be mentioned here and will not be considered as part of the separated beams.

Before analysis of the theoretical aspects of a multi-slit grating can be addressed, a few terms that will be used must be clarified. The term intensity is used to describe the flow of energy per unit area per unit time [Hecht & Zajac 1979]. In the lab one does not measure the intensity when using a device such as a photo detector to collect data. Instead, the time rate of flow of radiant energy or power is measured. The two are related by the fact that the intensity is equal to the power per unit area. Therefore, since they are directly proportional, all theoretical comparisons regarding the intensity correspond to the actual power measurements taken.

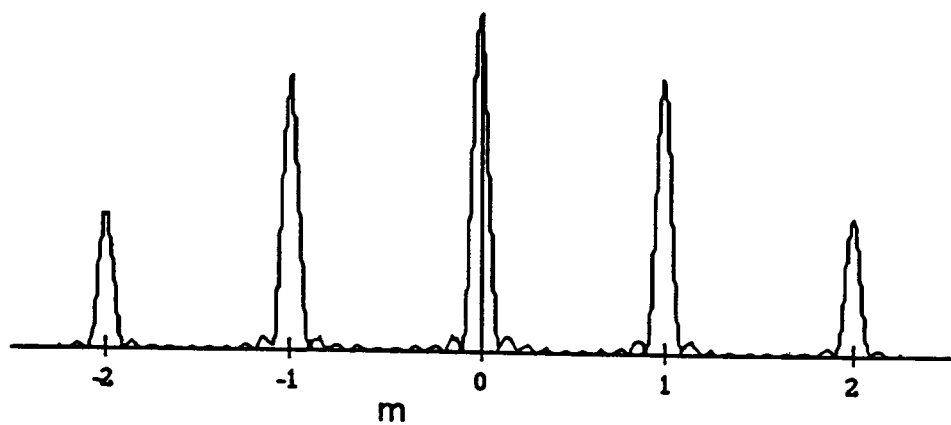


**Figure 2.1** Intensity pattern for a multi-slit grating. The standard ordering of principal maxima ( $m$ ) is shown.

## 2.2 How the Three-Grating Interferometer Works

The three-grating interferometer consisted of three amplitude gratings which were similar to Ronchi rulings (gratings with only a few lines per millimeter). A helium-neon laser was used as the source beam for the interferometer. Many diffraction orders were produced at each grating interface. Only certain orders of the diffracted beam at each grating were allowed to proceed through the three gratings (see Figure 1.1). The unwanted orders were blocked by the use of a pinhole or slit to allow only the desired 0th and 1st order beams to propagate and recombine. With the gratings positioned equidistantly, the two interfering beams from the second grating formed a sinusoidal pattern at the position of the third grating with a spacing equal to the spacing of the gratings. When the third grating was translated perpendicular to the grating lines, it alternately aligned the pattern created by the interfering beams with the grating lines. This gave a sinusoidal modulation after the third grating and from this a contrast ratio was calculated using the following formula,

$$\text{contrast ratio} = (I_{\max} - I_{\min}) / (I_{\max} + I_{\min}) \quad (2.4)$$

where  $I_{\max}$  was the maximum signal and  $I_{\min}$  was the minimum signal. A large contrast ratio (.5 or better) signified good alignment of the three gratings. Measuring the contrast was a simple way to test the three-grating interferometer and will be used in the following discussion on rotational and translational constraints.

The three-grating interferometer we initially used in our experiment had gratings with 79 lines/cm and only the 0th and 1st order beams were used. It was important to understand how much power was transmitted in each beam at the different grating interfaces. This was a difficult task to treat theoretically so actual measurements were taken to give insight as to how much power

remained after the third grating. The beam path is shown in Figure 1.1 where the incident beam is separated into paths A and B at the first grating and these two beams generate paths C and D at the second grating which recombine at the third grating creating paths E and F. Initially power readings were taken after the first grating of the 0th and 1st order (paths A and B) and were compared to the input power. The input power ( $I_{in}$ ) was 2.84 mw which gave a 0th order power ( $I_0$ ) of .38 mw and a 1st order power ( $I_1$ ) of .22 mw. Thus the ratio of intensities  $I_0/I_{in}$  was .13 for the 0th order beam and  $I_1/I_{in}$  was .08 for the 1st order. The modulated output after the third grating can either be measured from path E or F, but it was found that there was only a slight variation in the contrast ratio. For path F, a maximum ( $I_{max}$ ) was measured to be  $7.5 \mu\text{w}$  with a minimum ( $I_{min}$ ) of  $1.3 \mu\text{w}$  which gave a contrast ratio of .70 and ratios of  $I_{max}/I_{in}$  and  $I_{min}/I_{in}$  of  $2.6 \times 10^{-3}$  and  $4.6 \times 10^{-4}$  respectively. The expected output of the atomic interferometer can be predicted by assuming the gratings are similar to those described by Keith *et al.* [1988] which would give a final output of approximately  $3 \times 10^{-3}$  of the input and is consistent with the measurement of the optical three-grating interferometer.

## 2.3 Alignment Specifications

### 2.3.1 Separating the Correct Beams

In order to ensure that you were observing the output at the third grating from only the desired ordered beams, a technique was developed to make it easy to choose the correct orders. This may seem like a trivial task, but since there are many diffraction orders produced at each grating and they are only separated by a few millimeters, it can get confusing. At this point a detailed description of the experimental set-up needs to be mentioned. The three-grating interferometer consisted of three gratings with 79 lines/cm. The grating

line spacing  $a$  was  $1.27 \times 10^{-4}$  cm/line and the line width  $b$  was  $6.55 \times 10^{-5}$  cm, if the gratings were truly 50/50 gratings (see Figure 2.3). The gratings were mounted in mirror mounts to allow for ease in alignment and placed 38 cm apart on an optical bench. Pinholes were used in front of each grating to allow only the desired orders to proceed through to the next grating and to collect only the desired recombined output.

The following procedure was designed to ensure that only the correct ordered beams were used. The position of the pinhole in front of the third grating was the most crucial one as this was the position of the recombined output you wanted to observe. The input beam was diffracted at the first grating and the desired orders were allowed to proceed through. Path A (see Figure 1.1 for reference to beam paths) from the first grating was blocked in front of the second grating and the pinhole in front of the third grating was placed in front of path D. To make sure that the correct order had been chosen, path B was blocked in front of the second grating and the pinhole in front of the third grating was checked to see that it was indeed in line with path C. This ensured that

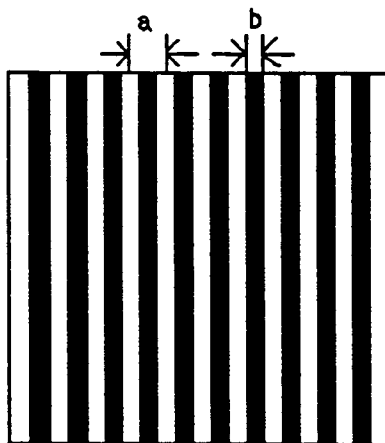


**Figure 2.2** A multi-slit diffraction grating. The grating spacing  $a$  and the metal grating line width  $b$  are shown. The grating is said to be 50/50 (50% transmission) when  $b=a/2$ .

only the -1st order and the +1st order maxima generated at the second grating from the 0th order and -1st order maxima generated at the first grating were recombined at the third grating.

The pinhole in front of the second grating was then opened only enough to allow the correct two orders (path A and B) through, blocking off all other orders. A pinhole was placed in front of the third grating which was opened only enough to allow the recombined orders (path C and D) through. This alignment procedure is fairly simple to accomplish, but must be done properly if the three-grating interferometer is to operate as it is intended to.

### 2.3.2 Grating Separation and Rotation Limitations

The three-grating interferometer is intended to be used as a measuring device, thus its stability and repeatability are important. It has four degrees of freedom; one translational in the z-direction and three angular (see Figure 2.4). The grating separation and rotation about each axis must meet certain criteria for proper alignment.

The grating separation of the three-grating interferometer is one aspect of the design of the system. The gratings must be separated by the same distance in order for the interferometer output to be optimized. A depth of field of  $\Delta z$  is associated with the sinusoidal grating pattern at the third grating. It is simply the range in which the pattern can be observed without washing out. It is related to the grating spacing  $a$ , the bandwidth of the source  $\Delta\lambda$ , and the collimation angle  $\Delta\theta$  by the following equation [Chang *et al.*, 1975]

$$\Delta z = \frac{a^2}{\Delta\lambda} \quad \text{or} \quad \frac{a}{\Delta\theta} \quad (\text{which ever is smallest}). \quad (2.5)$$

This leads to restrictions of the grating spacing which can be very small. For our experiment  $\Delta\theta$  was 1.35 mrad (from the HeNe laser specs). Since the light

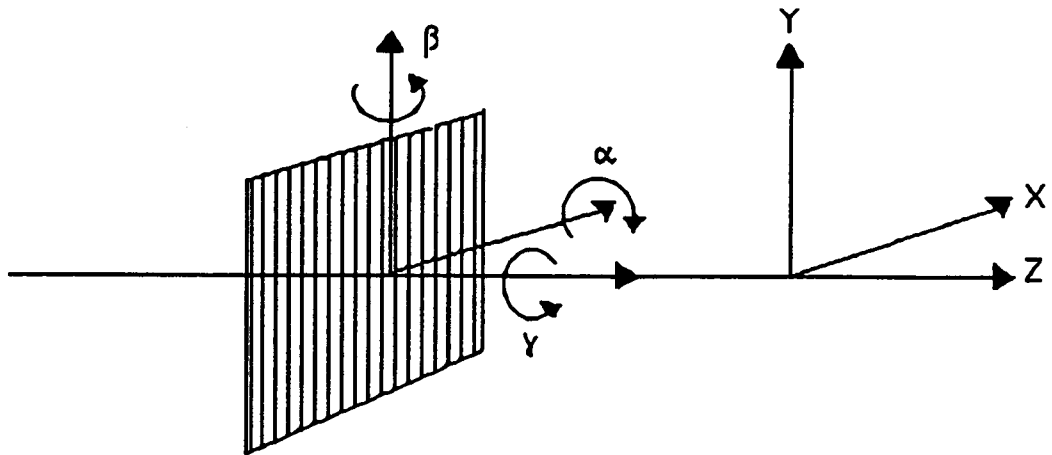


**Figure 2.3** Rotation angles for the three degrees of freedom. The rotation about the x axis is designated by the angle  $\alpha$ , about the y axis  $\beta$ , and about the z axis  $\gamma$ .

source used was monochromatic,  $\Delta\lambda$  was very small. Thus the equation using  $\Delta\lambda$  in the denominator would be very large so can be ignored. This gave a grating separation limitation of

$$\Delta z = \frac{a}{\Delta\theta} = \frac{1.27 \times 10^{-4} \text{ cm}}{1.35 \text{ mrad}} = 9.4 \text{ cm.} \quad (2.6)$$

This determines the distance by which the gratings can be misaligned and is not difficult to accomplish.

To test this result the second grating of the three-grating interferometer was moved in the x-direction with a stepping motor to measure the maximum and minimum power (i.e. intensity) and calculate a fringe contrast ratio as the third grating was translated in the z direction. Moving the second grating with a stepping motor generated a sinusoidal pattern that had double the frequency of the sinusoidal pattern created by moving the first or third grating which was due to a factor of two which appears in the phase shift of the two beams at the

second grating. The contrast ratio was used as a way of determining when the limit had been reached. Figure 2.5 shows the results of these measurements and agreed well with the calculated depth of field.

Rotation about the x axis is restricted by the depth of field  $\Delta z$  and the height of the beam h. In order to maintain a good contrast, the grating must be within the depth of field. Thus the restriction on the rotation angle about the x axis is given by

$$\alpha = \frac{\Delta z}{h}. \quad (2.7)$$

For our experimental set up  $\Delta z = 9.4$  cm and the height of the beam was measured to be  $h = 2$  mm. This gave an  $\alpha$  of 4.7 radians. This implies that rotation about the x axis is not a major concern and thus experimental verification was not necessary.

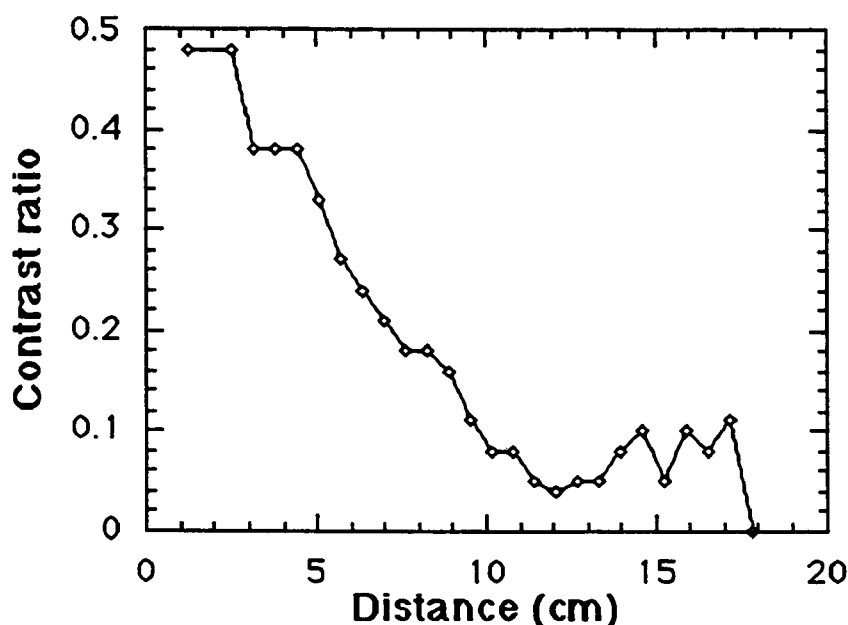


**Figure 2.4** Z axis translation of the third grating. The contrast ratio changes as the distance between the gratings is increased.

An alignment of the gratings that is slightly more difficult to obtain is the rotation about the y axis. This rotation will cause the grating spacing to be skewed to  $a/\cos(\beta)$  and must be limited by at most half a cycle over the beam width to avoid fringe washout. Rotation about the y axis is restricted by

$$\beta = \sqrt{\frac{a}{w}} \quad (2.8)$$

where  $w$  is the width of the beam and  $a$  is the grating separation. In our experimental set up  $a$  was  $1.27 \times 10^{-4}$  and  $w$  was assumed to be the same as  $h$  (since the beam was circular) so  $w = 2$  mm. Thus,  $\beta = .25$  radians or 14.4 degrees. This is a more strict task to accomplish but not impossible. In order to test this rotational alignment criteria, the third grating was rotated on the mirror mount and the contrast was again measured to determine if this equation holds true. The angle of rotation was measured with a simple protractor and thus was not very accurate. However, Figure 2.6 shows that the data obtained agrees fairly well with the calculation for the y axis rotation.

The most restrictive aspect of alignment is the alignment of the gratings about the z axis (how parallel the grating lines are with respect to each other). The angle of rotation about the z axis can be calculated using the following formula

$$\gamma = \frac{a}{2h}. \quad (2.9)$$

Using the values for  $a$  and  $h$  as before,  $\gamma = .03$  radians or 1.8 degrees. This is the alignment restriction which is most important, so mounting of the gratings with the grating lines as parallel as possible is the most important alignment feature. Due to the lack of the proper mounting device which could be rotated about the z axis, this equation was not verified. However, a technique that can

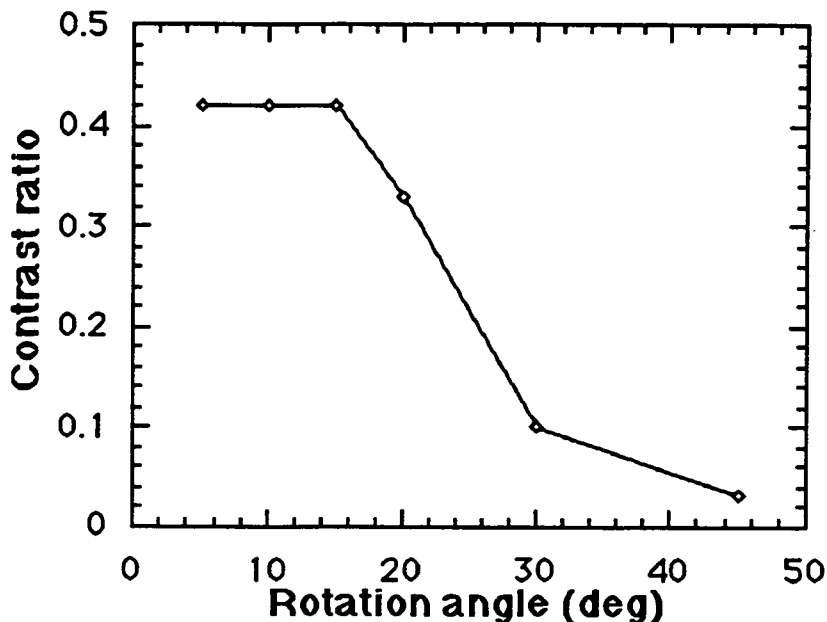


**Figure 2.5** Y axis rotation ( $\beta$  rotation) limitations. The contrast ratio is measured as the angle is increased.

be employed with the atomic gratings uses the optical polarization properties of the gratings to accomplish this alignment [Anderson *et al.*, 1988].

The restraints described in this chapter have proven to be fairly accurate (at least the ones tested). Therefore, they can be used when determining the conditions for proper alignment of the atomic gratings. The limitations on translation and rotation will be much smaller on the atomic scale. The atomic gratings that will be used in our experiment will have a grating spacing of 250 nm and will be separated by 5 cm. The atomic beam will be collimated using two 50  $\mu\text{m}$  slits placed 20 cm apart giving a  $\Delta\theta$  of 0.5 mrad. The height and width of the beam will be determined by the size of the grating substrates which will be 100  $\mu\text{m}$ . The spectral bandwidth of the atomic beam will be 0.01 nm. Using these values, the following criteria will be necessary for proper alignment of the atomic gratings. The limiting values are; for  $\Delta z$ , 0.5 mm; for  $\alpha$ , 5 rad; for

$\beta$ , 50 mrad; and for  $\gamma$ ; 1.2 mrad. By using the criteria equations to determine the limits of the three-grating atomic interferometer, it becomes obvious how important they are.

## Chapter 3

### Stabilization Using a Servo System

#### 3.1 Stabilization Criteria

The main purpose of this thesis is to provide a method for stabilizing an atomic interferometer. Low frequency noise is easily reduced with the aid of a servo system. One goal was to determine how much the gratings actually moved due to noise with the servo circuit on and off. This gives us a limiting value for the movement of the gratings in the x-direction.

Since the three-grating optical interferometer will eventually be used in conjunction with an atomic interferometer, it must be vibration-isolated. The atomic interferometer will be mounted along side the optical version on a single structure which will incorporate passive stabilization techniques. In order to achieve active vibration isolation, a servo system will be attached to the three-grating optical interferometer. During the data collection interval, the interferometer output must not move from maximum to minimum. In order to avoid washing out of the fringes formed at the third grating, the second grating will need to be stabilized in the x-direction utilizing the servo system.

#### 3.2 The Servo System

Before the servo system was employed, the three-grating interferometer was reconfigured with more stable mounts and gratings with 200 lines/mm in order to spread out the 0th and 1st orders. The three gratings were placed in machined aluminum plates with holes of proper width to allow only the two orders to proceed through to the third grating. A simple paper pinhole was placed over the third grating to capture only the recombined output. Figure 3.1 shows a diagram of the servo system. The HeNe laser generated the optical beams which were separated and recombined at the third grating. A photo

diode was placed behind the third grating and then connected to the input to the servo circuit. Channel one of the oscilloscope was connected to the offset monitor of the servo circuit which was the input amplified by a gain factor of two. After initial adjustments using the oscilloscope, the offset monitor signal was connected to the computer for data retrieval and analysis. The integrated output from the servo circuit was then connected to the input of the high voltage amplifier. The high voltage amplifier was monitored to observe the output of the servo circuit on channel two of the oscilloscope. The second grating of the interferometer was fitted with two piezoelectric devices (PZT's) placed back to back for maximum movement in the x-direction of the gratings and a micrometer for manual adjustments. The PZT's were driven by the high voltage power amplifier. When everything was properly aligned and adjusted, you could tap on the optical bench and view the noise created on channel one as a short lived ringing pattern.

The PZT's had a resonance at approximately 160 Hz, thus the region for which the servo system worked best was in the low frequency range. There are other frequencies that were hard to get rid of (60 Hz for instance), but they will be dealt with in other ways like shielding or isolating electronic offenders. The servo circuit was designed by a fellow graduate student and was used often by other members of our group. A few modifications were made to optimize its output and stability (see Figure 3.2). The capacitor on the integrator ( $C_{out}$ ) was chosen to maximize the gain of the servo circuit . When the initial design of the servo circuit was tested, a signal generator was used at different frequencies to test the frequency dependence of the servo circuit and the PZT's. Each had its own inherent problems; the PZT's were limited in movement, and the servo circuit began to oscillate above a certain frequency. A slight phase shift was

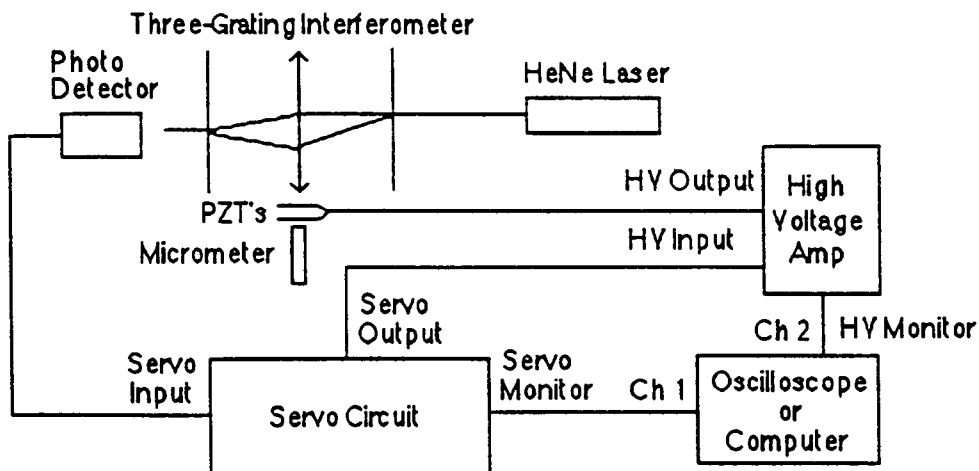


**Figure 3.1** Diagram of the three-grating interferometer servo system.

observed in the output at about 160 Hz due to the PZT's resonance, and thereafter the output continued to shift in phase until there was a 90 degree phase shift at or near 250 Hz. This limiting frequency was where the servo circuit began to oscillate.

One main problem with the servo circuit was getting it to "lock" meaning that the output would properly compensate for any input fluctuations. A few points will be mentioned on how to properly adjust the servo circuit components in order to obtain a good locked signal for data analysis. First a sine wave input was applied to the high voltage input to adjust the dc offset of the signal. The offset monitor signal was centered around the middle of the sinusoidal max and min by manually adjusting the position of the second grating with the micrometer. When the servo circuit was turned on, the output tried to correct for any deviation of the input away from the zero of the sinusoidal pattern. The optimum locking position is shown in Figure 3.3 a. The servo circuit generates an error signal which only works when the three-grating interferometer output (servo input) is locked near the maximum positive (or negative) slope of the sine

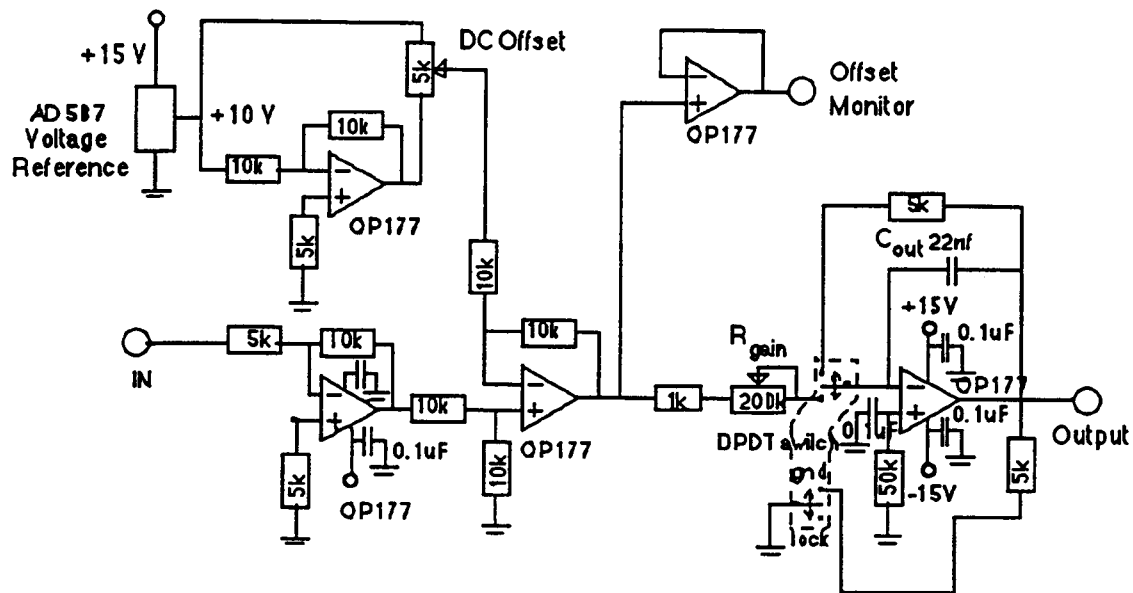


**Figure 3.2** Schematic diagram of the servo circuit.

wave pattern. When the servo circuit became unlocked, the offset monitor signal jumped to a constant dc level. Figure 3.3 c and d show how the signal becomes distorted when moved away from the central dc offset position. Once the dc offset pot and alignment were set, the servo system was fairly stable and only needed minor adjustment to reproduce locking from day to day.

The servo circuit was very sensitive to the gain of the rest of the system. If the gain decreases/increases out of the range for adjustment on the 200k pot, then you could not reproduce locking from day to day. The 200k pot ( $R_{gain}$ ) was initially set in the middle of its range to allow for adjustment to either side. Tweaking  $R_{gain}$  until the servo system started to go into oscillation and then backing off slightly gave the best results with maximum gain. Minor adjustments to the servo system were needed before each data collection to optimize the locking position.

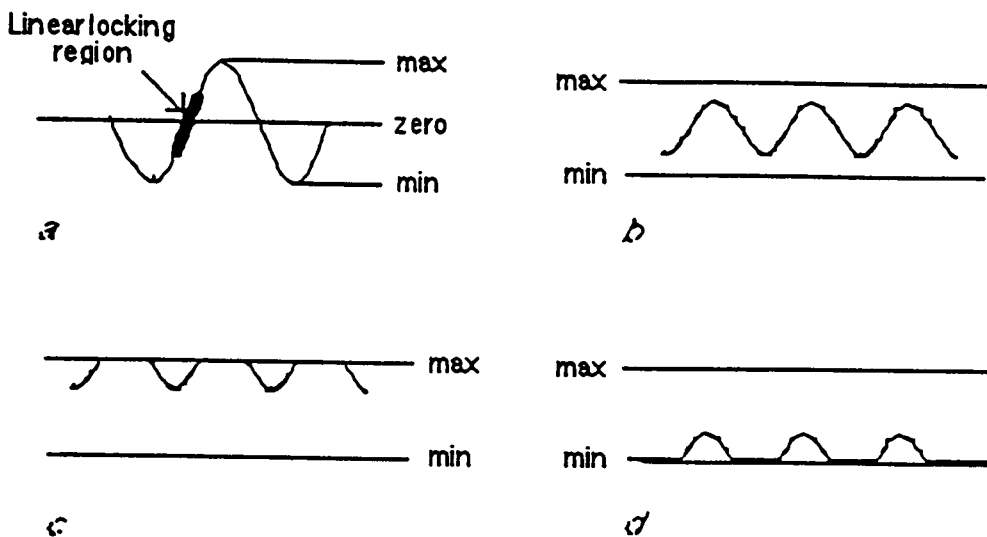


**Figure 3.3** Pictorial view of the servo circuit locking technique. In *a*, the optimum locking position is shown. The sine wave is created by moving the grating by hand or with a signal generator. In *b*, the monitor voltage (or noise) is centered in the middle of the sine wave max and min. Improper adjustment is shown in *c* and *d*, where clipping occurs when the monitor voltage is tweaked away from the central dc offset.

## Chapter 4

### Results of Stabilization

#### **4.1 Data Acquisition Techniques**

The output of the servo system was small in size ( $\sim .1$  volt) and had to be amplified before collecting data on the computer. For data analysis, a Mac IIci computer was used, utilizing the appropriate software programs. The offset monitor from the servo circuit was fed through a Tektronix differential amplifier into an A/D converter before proceeding to the computer. The differential amplifier had a filter which was used to select the noise range below 1 kHz. A data acquisition program called "Superscope" was used to plot the output signal from the servo system and observe it in "real time". This program allowed you to use the computer as an oscilloscope and save data. Another software program that was used for plots was "Kaledigraph". A data manipulation program called "Maple" was also used to perform calculations on the data. Care must be taken when determining the actual movement of the grating, as many scaling factors must be included. The servo offset monitor signal was simply a voltage that fluctuated with movement of the second grating. The noise signal is shown in Figure 4.1 when the servo circuit is turned on and off. This noise was then manipulated using fourier transforms and Parseval's theorem to determine the frequency spectra that existed in the noise signal. In this way, the frequencies that were quenched using the servo system were easily detectable.

#### **4.2 Analysis of the Noise**

The offset monitor signal was fed to the computer and produced a voltage  $V(t)$ . The sampling interval  $\Delta t$  was .5 ms for  $N = 16,384$  data points giving a total time for data collection of  $T = 8.2$  seconds. We would like to know

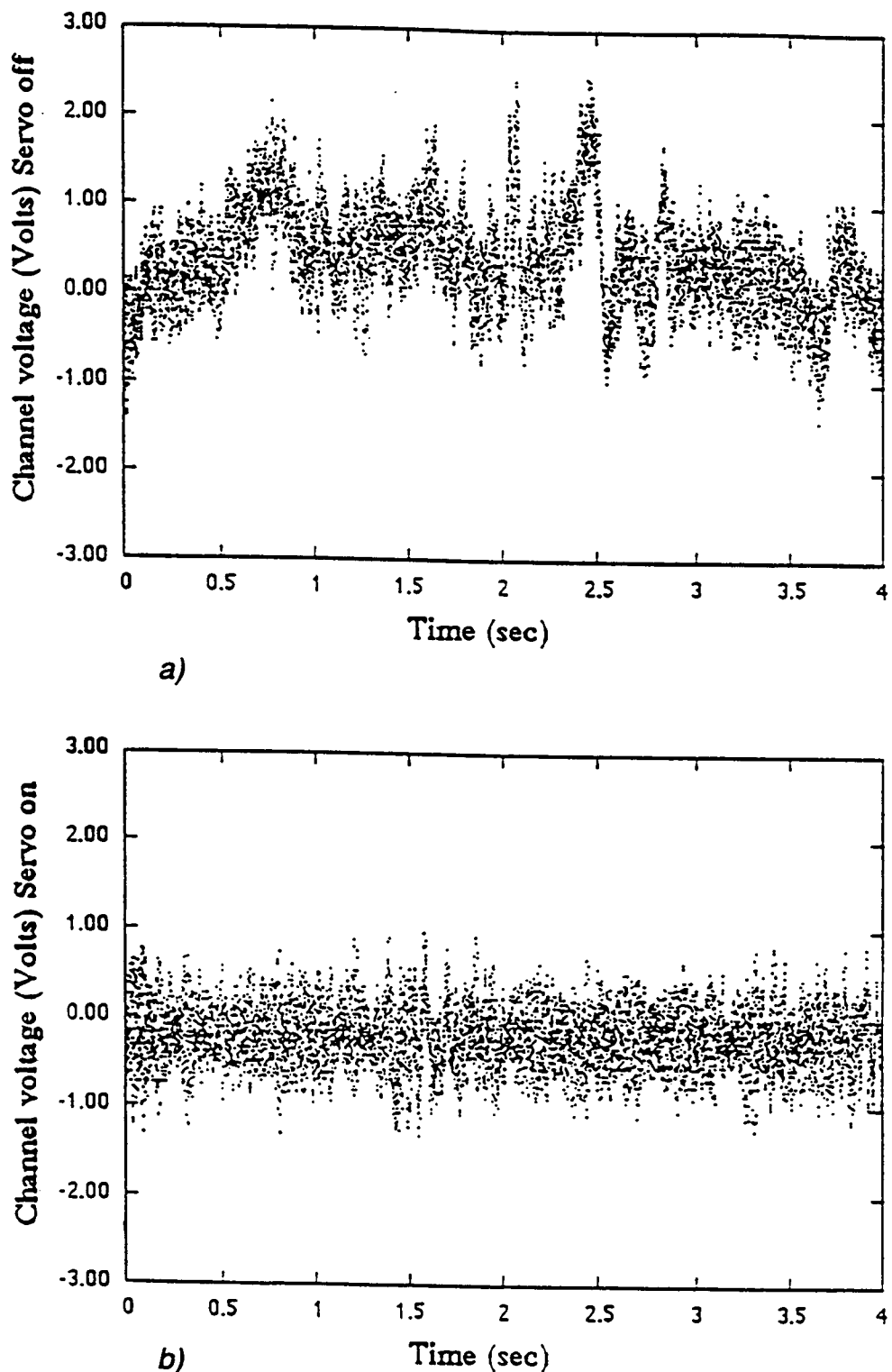


**Figure 4.1** Servo circuit offset monitor signal where in *a* the servo circuit was turned off and in *b* the servo circuit was turned on.

how the root mean square voltage ( $V_{\text{rms}}$ ) and the standard deviation ( $V_{\text{std}}$ ) depends on frequency and relate this to actual movement of the gratings. A correction factor from volts to distance moved by the gratings must be calculated. The input signal (as seen at the offset monitor) was a function of the movement in the x-direction and is given by

$$V(x) = \frac{V_{\text{mon}}}{2} \sin\left(\frac{2\pi x}{\frac{a}{2}}\right) \quad (4.1)$$

where  $V_{\text{mon}}$  was the voltage at the offset monitor and  $a/2$  was used due to the factor of two in the phase when moving the middle grating. We can take the derivative with respect to  $x$  and then choose  $x=0$  for convenience to get

$$\frac{dV}{dx} = \frac{4\pi}{a} \frac{V_{\text{mon}}}{2} = \frac{2\pi V_{\text{mon}}}{a} \quad (4.2)$$

which can then be inverted to give a scaling factor which also includes a factor for the gain of the amplifier to the computer ( $G_{\text{amp}}$ ) of

$$\text{scaling factor} = \frac{dX}{dV} \frac{1}{G_{\text{amp}}} = \frac{a}{2\pi V_{\text{mon}} G_{\text{amp}}} . \quad (4.3)$$

This scaling factor will be used to convert  $V_{\text{std}}$  to the distance the second grating has moved in the x-direction ( $D_{\text{std}}$ ).

### 4.3 Low Frequency Noise Reduction

Another important aspect to investigate was to determine the frequencies in the noise signal. A fast fourier transform (FFT) of the signal can give valuable insight into the frequencies involved in the noise. In order to correctly analyze the data and make sure all scaling factors were included, Parseval's theorem was used. Simply stated it says that "the power in the time domain is equal to the power in the frequency domain" [Hecht & Zajac, 1979]. We want to relate

the  $V_{rms}^2$  or the power in the time domain to the power spectral density (PSD) or power in the frequency domain.  $V_{rms}$  is given by [Press *et al.*, 1986]

$$V_{rms} = \sqrt{\frac{1}{T} \int_0^T |V(t)|^2 dt} \quad (4.4)$$

Using Parseval's theorem, we have the following relationship

$$\frac{1}{T} \int_0^T |V(t)|^2 dt = \int_0^{f_c} PSD(f) df \quad (4.5)$$

where the Nyquist frequency  $f_c$  is  $1/2\Delta t = 1$  kHz. The FFT was calculated on Maple and related to the PSD with proper scaling factors by

$$PSD = \frac{T}{2} |\text{FFT}|^2 \quad (4.6)$$

with units of  $V^2/\text{Hz}$ . The data was transferred to Kaledigraph for plotting. Figure 4.2 plots the PSD as a function of frequency for different ranges using the scaling factor to give the proper units. It shows the frequencies that were present in the servo system and therefore the three-grating interferometer. The system had a resonance at around 160 Hz. The 60 Hz noise (and multiples thereof) were not eliminated significantly by the servo system. The frequency spectra in Figure 4.3 *a* and *b* show the frequencies that are present when the servo circuit is on and off. The servo system was very effective up to about 10 Hz. The noise in this frequency range was reduced by at least a factor of 10. At 1 Hz, the servo system had succeeded in reducing the noise by 95%, and was still 75% effective at 10 Hz. The data showed the reduction in low frequency inertial noise where it is most needed in the three-grating interferometer.

The most important calculation was using the  $V_{rms}$  to obtain  $V_{std}$  with the scaling factor to calculate the distance traveled by the second grating when the

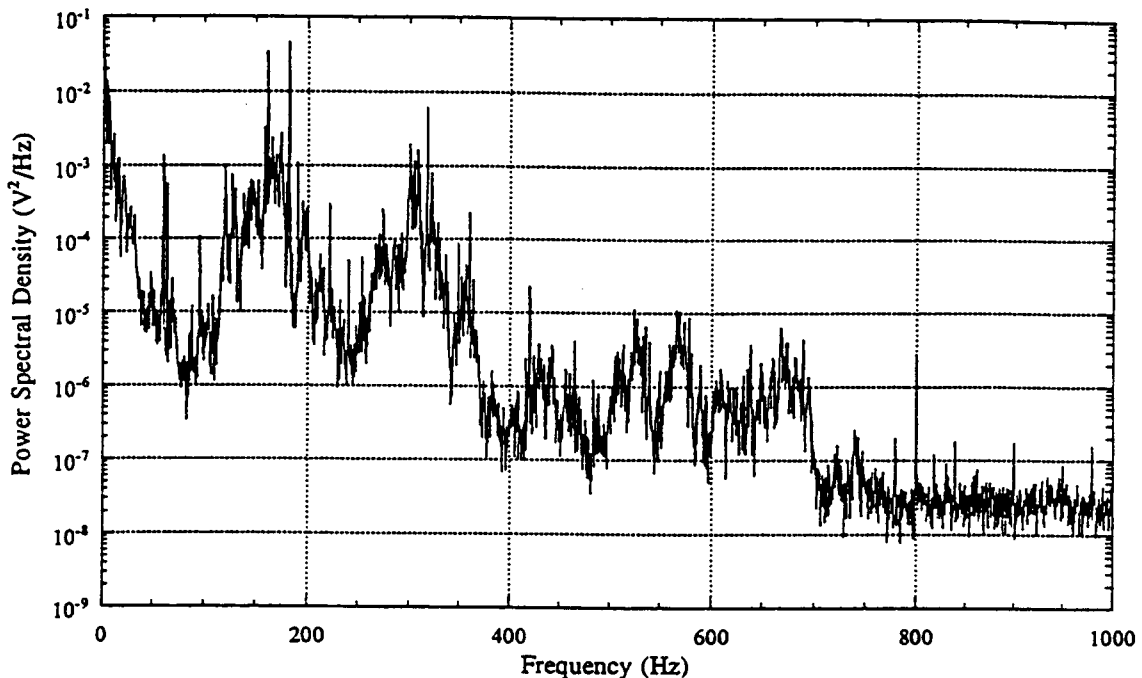
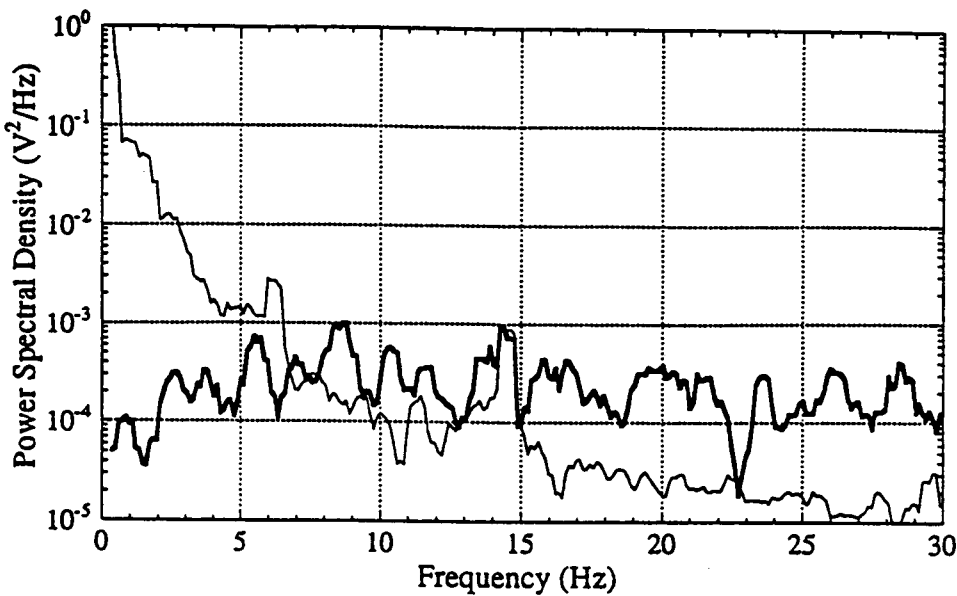
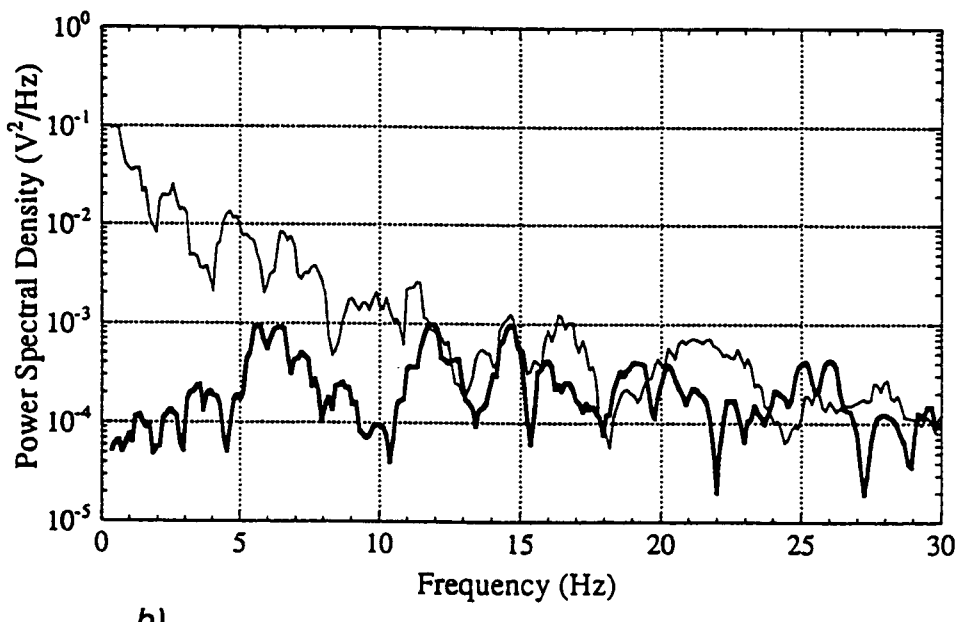


**Figure 4.2** Frequency spectra of the servo system output. The range of frequencies in the noise signal is shown up to 1000 Hz.

servo circuit was on and off. Maple was used to calculate  $V_{std}$  for the servo circuit on and off and then the scaling factor takes the data from volts to nanometers. Data was collected on two separate data acquisitions as shown in Figure 4.3 and the best results were used for the calculations of  $V_{std}$ . The results were  $V_{std(on)} = .431$  V and  $V_{std(off)} = 1.057$  V giving a distance traveled for each of  $D_{std(on)} = 3.1$  nm and  $D_{std(off)} = 7.7$  nm. This clearly shows the effectiveness of the servo system in terms of how much movement occurred and was suppressed at the second grating of the three-grating interferometer.



a)



b)

**Figure 4.3** Frequency spectra with the servo circuit on and off. The reduction in noise is displayed in *a* and *b* for two separate data collections with the normal line corresponding to when the servo system was off and the bold line corresponding to when the servo system was active.

## Chapter 5

### Conclusions

The three-grating optical interferometer was thoroughly investigated so as to better understand how the atomic interferometer will work with laser cooled atoms. The path that the atomic beam will take was described and measurement of the expected output taken to allow estimates to be made of the atomic beam output. Since the beam went through three gratings before being detected and measured, there was a lot of loss in the intensity. Less than 1% of the input beam can be expected to be detected behind the third grating. This may seem like a small amount, but the atomic beam strength should be large enough that there will be a sufficient supply of atoms proceeding through the third grating.

Another aspect that might affect the final output is the alignment of the three gratings. The criteria developed were tested and proved to be in good agreement with the limiting equations used. The translational and rotational restrictions can be applied to the atomic beam to determine the constraints on the atomic interferometer. The alignment of the three-grating interferometer need only be done when initially setting up the experiment, and should remain stable over time. A periodic check would verify that the grating positions have not changed. It is important to use care and accuracy when developing mounts and stable structures for the three gratings to sit upon. The optical version of the three-grating interferometer will make it possible to easily test for proper alignment of the atomic interferometer.

To compensate for inertial noise due to low frequency vibrations, a servo circuit was employed in conjunction with the three-grating interferometer. The entire servo system was described in detail and tested for effectiveness. The

servo system worked well at low frequencies. Its limitations were in the fact that the servo circuit would not operate effectively above about 250 Hz and had trouble dealing with electronic noise such as 60 Hz. The PZT's used were restricted in movement and thus added another limitation to the system. Other motion devices may need to be tested with the servo circuit to find the most useful combination.

It was interesting to see what frequencies exist in inertial noise. This was shown in the graphs of the data collected. When properly manipulated and accurately scaled using FFT's and Parseval's theorem, the frequencies present in the noise signal could be seen. The effectiveness of the servo systems action was very evident in the graphs of the frequencies with the servo circuit on and off. Calculation of the scaling factor which translated volts detected at the servo circuit to actual movement of the grating gave an interesting insight as to how much the gratings were moving due to the noise and the servo system correction. The distance between the grating lines used in this part of the experiment was 5 mm while the distance the grating moved due to the noise was less than 10 nm. This shows that even a small movement of the grating could effect the stability of the final output of the three-grating interferometer.

Using the optical version of the three-grating interferometer for initial alignment and stabilization of an atomic interferometer is important. The atomic interferometer would be very difficult to align and monitor without it. The information presented in this thesis will hopefully be useful in developing an accurate detection device for laser cooled atoms. There are many other aspects of atomic and optical physics where the three-grating interferometer is useful. It could be used as a very sensitive rotational and gravitational sensor and improve the sensitivity of many experiments done in quantum optics. Thus, it is important to develop and utilize this new tool in atom optics.

## Bibliography

Anderson, E.H., Levine, A.M., and Schattenburg, M.L., *Appl. Opt.*, **27**, 3522 (1988)

Bonse, U. and Hart, M., *Appl. Phys. Lett.*, **6**, 155 (1965)

Chang, B.J., Alferness, R., and Leith, N.E., *Appl. Opt.* **14**, 1952 (1975)

Hecht, E. and Zajac, A., *Optics*, Addison-Wesley, Reading, Mass., 1979 pg. 344

Keith, D.W., Schattenburg, M.L., Smith, H.I., and Pritchard, D.E., *Phys. Rev. Lett.*, **61**, 1580 (1988)

Martin, P.L., Oldaker, B.G., Miklich, A.H., and Prichard, D.E., *Phys. Rev. Lett.*, **60**, 515 (1988)

Marton, L., *Phys. Rev.*, **85**, 1057 (1952)

Press, W.H., Flannery, B.P., Teukolsky, S.A., and Vetterling, W.T., *Numerical Recipes*, Cambridge University Press, New York, 1986 pp. 381-421

Rauch, H. *Helv. Phys. Acta*, **61**, 589 (1988)